ISSN 1392–1320 MATERIALS SCIENCE (MEDŽIAGOTYRA). Vol. 13, No. 3. 2007

Oxygen Isotopic Exchange On Three-Way Catalysts: A Dynamic Kinetic Model

Arvaidas GALDIKAS[1*], Daniel DUPREZ[2], Nicolas BION[2], Claude DESCORME[3], Teresa JUNEVIČ[1]

[1]*Physics Department, Kaunas University of Technology, 73 Donelaičio st., LT-3006 Kaunas, Lithuania*
[2]*Laboratoire de Catalyse en Chimie Organique (LACCO), UMR CNRS 6503, Université de Poitiers, 40, Avenue du Recteur Pineau, 86022 Poitiers Cedex, France*
[3]*Institut de Recherches sur la Catalyse (IRC), 2 avenue AlbertEinstein, 69626 Villeurbanne Cedex, France*

Received 29 May 2007; accepted 26 July 2007

A time-resolved kinetic analysis has been developed for modeling experimental results of $^{18}O/^{16}O$ isotopic exchange over oxide-supported metal catalysts. Model is based on two very important points: 1) the parallel calculation of surface and bulk diffusion and 2) the implication of certain O species such as superoxides. This model is based on rate equations and includes several elementary processes: adsorption on the metal nanoclusters, reactions on the metal nanoclusters, desorption from the metal nanoclusters, surface and bulk diffusion on/in the oxide support and direct exchange with the gas phase. On the basis of this model a computer code was developed to determine the kinetic and thermodynamic parameters of the oxygen isotopic exchange reactions. The characteristics of a Rh/CeO_2 and $Pt/Ce_xZr_{1-x}O_2$ catalysts were examined in the temperature range between 200 °C and 450 °C.

Keywords: catalysis, three-way automotive catalysts, surface diffusion, kinetics, isotopic exchange, oxide, kinetic modeling.

1. INTRODUCTION

To meet stringent regulations on exhaust emissions of spark-ignition engines, converters were progressively equipped with modern three-way catalysts (TWC) allowing to simultaneously convert unburnt hydrocarbons (HC), CO and NO_x (NO, NO_2,) to untoxic products H_2O, CO_2 and N_2 [1, 2]. The catalyst should be active under both oxidizing and reducing conditions. For that reason, ceria-based oxides must be used as supports [3]. Such supports may "absorb" the oxygen in excess and supply oxygen under reducing conditions. The oxygen mobility on the surface and in the bulk of such catalysts plays a major role in the catalytic process. To investigate the oxygen mobility and to better understand the oxygen pathways, oxygen isotopic exchange reactions were studied [4, 5].

On oxide-supported metals, $^{18}O/^{16}O$ exchange occurs through a sequence of well differentiated steps [6 – 9] as schematized on Fig. 1: 1) dissociative adsorption of $^{18}O_2$ on the metal nanoclusters; 2) transfer of ^{18}O atoms from the metal particles to the oxide surface; 3) migration of ^{18}O atoms on the oxide surface; 4) exchange between ^{18}O atoms and ^{16}O from the oxide. Furthermore, depending on the reaction temperature, two other steps might be encountered: 5) internal (bulk) migration and exchange of ^{18}O atoms with ^{16}O from the oxide bulk; 6) direct (non-dissociative) exchange between $^{18}O_2$ molecules from the gas phase and dioxygen species on the support.

Depending on the experimental conditions (e. g. the temperature), two exchange regimes are distinguished [10]: 1) homoexchange, when only oxygen atoms from the gas phase participate in the exchange processes. Oxygen atoms from the oxide do not participate. In this case the exchange processes exclusively take place on the metal particles. Homoexchange studies give profitable information on the oxygen activation step at the metal particles surface; 2) heteroexchange, when oxygen atoms from the oxide do participate in the reaction. In this case, pure $^{18}O_2$ is introduced into the reactor and the formation of $^{16}O_2$ and $^{16}O^{18}O$ is followed as a function of time. Heteroexchange studies give direct information about the kinetics of the oxygen transportation on the catalyst.

The aim of this paper is to present a real time kinetic model for analysis of oxygen isotopic exchange on powder TW catalysts. Model is based on two very important points: 1) the parallel calculation of surface and bulk diffusion and 2) the implication of certain O species such as superoxides. In these solids, the metal clusters act as porthole for oxygen exchange at the oxide surface and in the bulk. It is not possible to design specific experiments allowing to discriminate between the different steps of exchange. Therefore, the kinetic model should take into account all the elementary steps involved in the exchange process: adsorption, recombination and desorption on of binuclear oxygen species. Experimental kinetic curves of partial pressures of oxygen species $^{18}O_2$, $^{16}O_2$ and $^{18}O^{16}O$ in gas phase are first recorded in a close-loop reactor at temperatures ranging from 200 °C to 450 °C under reduced pressure (50 mbar). $Pt/Ce_xZr_{1-x}O_2$ (Fig. 2) and Rh/CeO_2 catalysts were used as model TW catalysts in this study. From the best fitting of these curves with the theoretical curves calculated by the kinetic model, information about elementary steps of oxygen exchange process can be obtained and the values of parameters such as reaction rate constants, surface and bulk diffusion coefficients and activation energies of these processes can be calculated. To follow the time dependencies of isotope composition on metal clusters and on the surface layers of oxide (including

*Corresponding author. Tel.: +370-37-300349; fax.: +370-37-456472.
E-mail address: *galdikas@ktu.lt* (A. Galdikas)

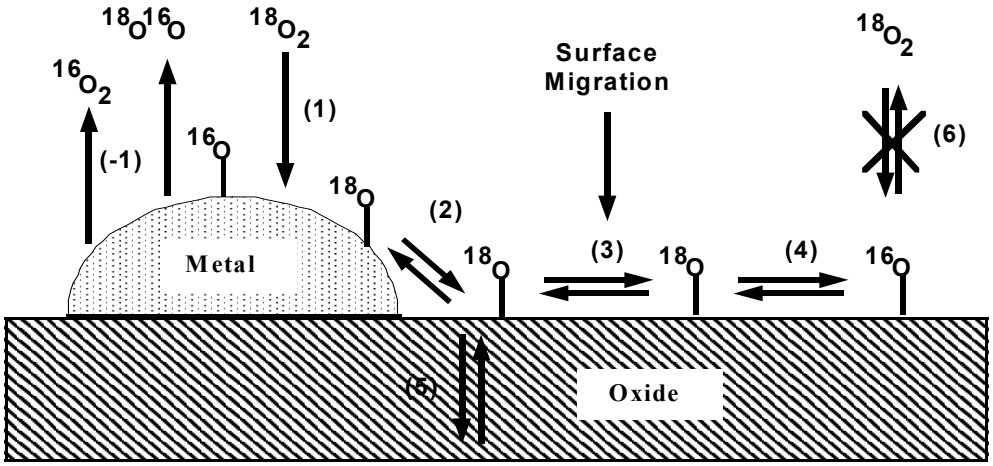

Fig. 1. Scheme of the isotopic exchange mechanism between $^{18}O_2$ (g) and ^{16}O atoms from the oxide over supported metal catalysts

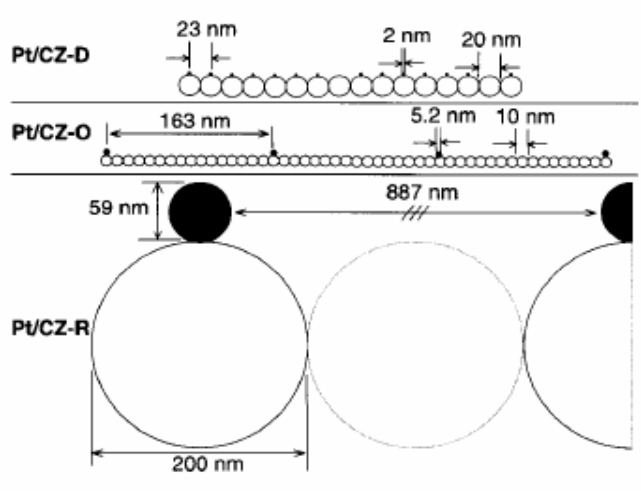

Fig. 2. Nanometric pictures of the three-way catalysts

deeper monolayers), atomic fluxes crossing the perimeter of metal clusters are calculated and analyzed. This allows us to get a deeper insight in all the steps of exchange process. On the basis of this model, a computer code is built for analysis of automotive catalysts.

2. EXPERIMENTAL

Oxygen isotopic exchange experiments were carried out on a ceria-supported rhodium catalyst (0.3 wt-% Rh/CeO_2, $S_{BET} = 27\ m^2g^{-1}$, average oxide grain size = 260 Å, average metal nanocluster particle size = 15 Å, dispersion = 56 %). About 20 mg of the catalyst were used for each experiment.

The oxide we used as a support, supplied by Rhodia Electronics and Catalysis (La Rochelle, France), was pre-calcined at 900 °C for 6 hours. The catalyst was then prepared at room temperature by impregnation of the support, in excess water, with an aqueous solution of rhodium nitrate ($Rh(NO_3)_3$). After drying overnight at 120 °C, the catalyst was calcined in dry air (30 mL min^{-1}) at 450 °C for 4 hours.

$Pt/CeZrO_2$ samples were synthesized as descried earlier in ref. [11], by high energy ball milling of CeO_2 and ZrO_2 powders and by conventional impregnation using metal clusters, surface and bulk diffusion and direct exchange on surface of support by participation $Pt(NH_3)_2(NO_2)_2$ as platinum precursor. Detail description of this experimental method is done in refs. [4, 10, 12].

The experimental setup consisted in a re-circulated gas manifold consisting in a tubular quartz reactor (Fig. 3), a re-circulating pump (Metal Bellows MB-41E) to circulate the gases over the catalyst and a mechanical pump to evacuate the system before and after each experiment [4, 10]. An efficient re-circulating pump, operating under reduced pressure (50 mbar), is necessary to avoid any diffusion and mass transport effects in the gas phase. Such a phenomenon would limit the changes in the partial pressures and then distort the results. $^{16}O_2$, $^{18}O_2$ and $^{16}O^{18}O$ were monitored using a Quadrupole Mass Spectrometer (QMS 420 Balzers) connected to the reaction loop via thermo-valve (Balzers RVG 050 A). This valve was calibrated so that the total pressure in the ionization chamber was kept constant at 10^{-6} mbar. For the reactions, pure gases were used: $^{16}O_2$ >= 99.995 % pure (Air Liquide, Alphagaz1) and $^{18}O_2$ >= 99 % pure (Isotec).

3. CALCULATION OF THE DIFFUSION COEFFICIENTS

When surface migration is the rate determining step in the oxygen exchange reaction, the surface diffusion coefficient might be calculated using a simple model developed by Kramer and André [4, 13]. This model assumes circular sources (metal nanoparticles) distributed on an infinite surface. Then, the amount of oxygen atoms diffusing on the support is given by:

$$N_e = \frac{2}{\sqrt{\pi}} C_m^{18} I_o \sqrt{D_s t} \qquad (1)$$

The initial slope (S_1) of the kinetic curve N_e vs. $\sqrt{t}$ gives the surface diffusion coefficient:

$$D_s = \frac{\pi}{4}\left(\frac{S_1}{I_o C_m^{18}}\right)^2$$

$$\text{with } S_1 = \left(\frac{dN}{d\left(\sqrt{t}\right)}\right)_{t=0} \qquad (2)$$

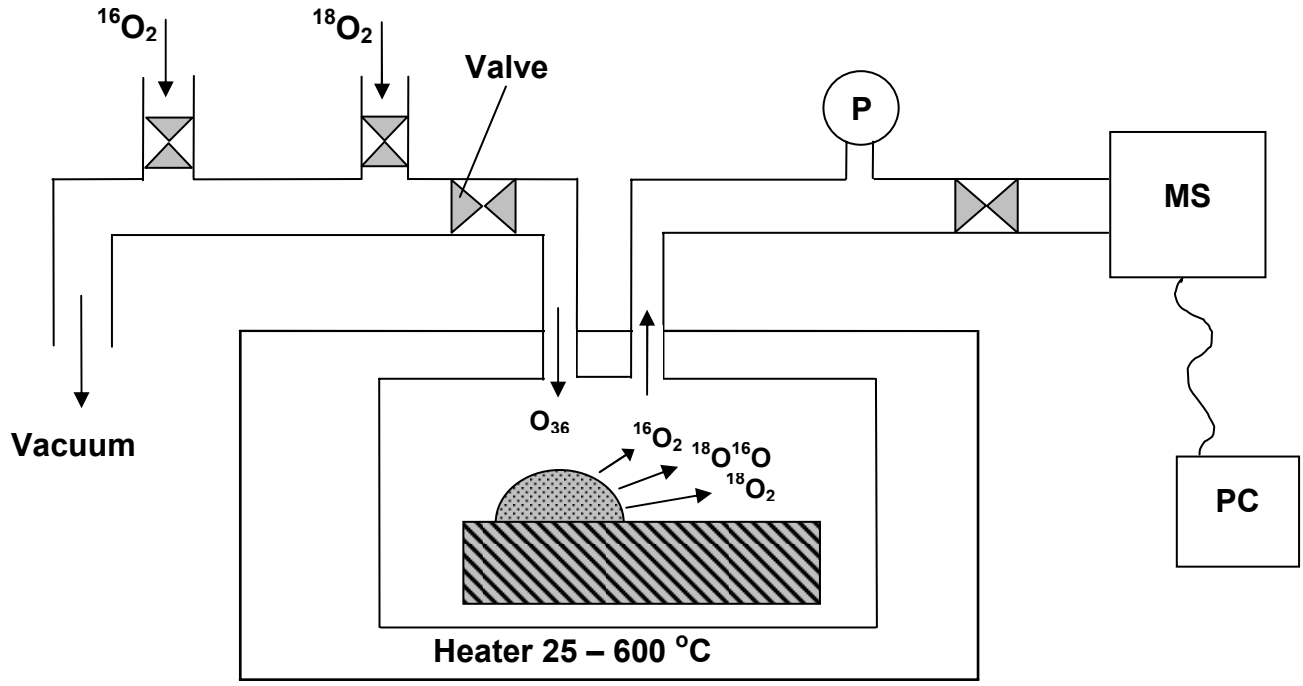

Fig. 3. Oxygen isotope exchange reactor (MS – Quadrupole Mass Spectrometer; PC – personal computer; P – pressure sensor)

and $I_o = \dfrac{\beta \cdot x_m D^2}{A}$,

where x_m is the metal loading in the catalyst (wt. %), D is the dispersion of the metal nanoparticles (%), A is the surface area of the catalyst ($m^2\,g^{-1}$) and β is the surface atomic concentration in metal nanoparticles (at m^{-2}).

When the support exhibits a significant internal mobility of oxygen, the bulk diffusion coefficient (D_b) might be calculated as follows, using a model developed by Duprez [4] and Kakioka et al. [14]:

$$-\ln\left(\frac{\alpha_g^t - \alpha_s^0}{\alpha_g^\infty - \alpha_s^0}\right) = \frac{\rho A}{N_g}\sqrt{\frac{4D_b t}{\pi}} \quad , \tag{3}$$

where ρ is the oxide density, N_g is the total amount of ^{18}O atoms in the gas phase and S_2 is the slope of the curve $-\ln\left(\left(\alpha_g^t - \alpha_s^0\right)/\left(\alpha_g^\infty - \alpha_s^0\right)\right)$ vs. $\sqrt{t}$. α_g^t, α_g^∞ and α_s^0 are respectively the atomic fractions in ^{18}O in the gas phase (g) and in the solid (s) at time zero, at time t and at the equilibrium (∞). Then, the bulk diffusion coefficient is expressed as:

$$D_b = \frac{\pi}{4}\left(\frac{S_2 N_g}{\rho A}\right)^2 \quad . \tag{4}$$

When the elementary processes (surface and bulk diffusion) are well separated, these equations allow us to calculate the diffusion coefficients fro wt-%m the kinetic curves. In that case, only the initial time of the exchange process is taken into account for the calculations. Experimental curves cannot be fitted this way.

However, only the fitting of the entire experimental kinetic curves can indicate which elementary processes take place and which one is dominating upon catalysis. For that reason a kinetic model had to be developed for a better understanding of the reaction schemes upon exchange on ceria-based mixed oxides with high oxygen mobility.

4. KINETIC MODEL

4.1. Exchange on the Metal Nanoclusters

Generally, oxygen exchange on metal nanoclusters proceeds in three steps: 1) adsorption of dioxygen molecules and dissociation, 2) reaction between oxygen atoms and formation of dioxygen molecules and 3) desorption of dioxygen molecules to the gas phase. The third one is not a limiting step as the activation barrier for desorption of molecular dioxygen is low. As a result, it is assumed that dioxygen molecules formed on the metal surface immediately leave the surface. The time variation of the concentration in the gas phase of the i-th type of dioxygen molecule consists of two terms: the adsorption and the chemical reactions contributions.

$$\frac{dn_i}{dt} = \left(\frac{dn_i}{dt}\right)_{Ad} + \left(\frac{dn_i}{dt}\right)_{\mathrm{Re}} \quad . \tag{5}$$

For the kinetic modeling of the surface processes [15], the adsorption term is usually represented by the Langmuir-Hinshelwood equation:

$$\left(\frac{dn_i}{dt}\right)_{Ad} = \alpha_i I_i c_m \quad , \tag{6}$$

where α_i is the sticking coefficient, I_i is the flux of particles to the surface, c_m is the relative atomic concentration of metal atoms in the first atomic layer at the metal nanoparticles surface. This concentration decreases when the coverage in adsorbed oxygen isotopes (^{18}O and ^{16}O) increases. In fact, $c_m + c_{16} + c_{18}$ is kept equal to 1.

The flux of particles arriving to the surface is estimated from the expression:

$$I_j = p_j N_A \left(2\pi M_j RT\right)^{-1/2} ,$$

where p_j is the partial pressure of the j-th type species, M_j is molecular mass of the j-th type species and N_A is the Avogadro number.

The sticking coefficient for oxygen on noble metals (Pt, Pd, Rh, Ir, Ru) is close to 1.

In our case, the oxygen flux to the surface at 50 mbar is so high that the metal nanoclusters were considered as fully covered by oxygen atoms even at the very beginning of the experiment. Consequently, the oxygen isotopic composition on the metal surface was considered to be equal to the oxygen composition in the gas phase. Then, before each iteration during the calculation, the surface composition of the metal nanoclusters is obtained from the following expression:

$$\begin{cases} \left(\Delta c_{16}(t)\right)_{AD} = \left(f_{32}(t) + \frac{1}{2} f_{34}(t)\right)\left(c_m - (c_{16}(t) + c_{18}(t))\right) \\ \left(\Delta c_{18}(t)\right)_{AD} = \left(f_{36}(t) + \frac{1}{2} f_{34}(t)\right)\left(c_m - (c_{16}(t) + c_{18}(t))\right) \end{cases}, \quad (7)$$

where $f_i(t)$ is the fraction, at time t, of the i-th type of oxygen isotope in the gas phase. The term in brackets gives the uncovered metal surface at time t after desorption of the dioxygen molecules (reaction).

The reactions between oxygen atoms taking place on the metal surface are as follows:

$$\begin{aligned} &^{16}O + {}^{16}O \rightarrow {}^{16}O_2 ; \\ &^{18}O + {}^{18}O \rightarrow {}^{18}O_2 ; \\ &^{16}O + {}^{18}O \rightarrow {}^{16}O{}^{18}O. \end{aligned} \quad (8)$$

The time variations of the oxygen atoms concentrations at the metal nanoclusters surface, according to the mass action law, are expressed as :

$$\begin{cases} \left(\frac{dc_{18}}{dt}\right)_{\mathrm{Re}} = -kc_{18}\left(\frac{1}{2}c_{18} + c_{16}\right) \\ \left(\frac{dc_{16}}{dt}\right)_{\mathrm{Re}} = -kc_{16}\left(\frac{1}{2}c_{16} + c_{18}\right) \end{cases}. \quad (9)$$

In the last equations, the factor of 1/2 accounts for the adsorption and the subsequent dissociation of the $^{16}O^{18}O$ molecules from the gas phase. In fact, as far as atomic concentrations are considered, and not molecular concentrations, a factor of 1/2 is need. After dissociation, one $^{16}O^{18}O$ molecule gives only one ^{16}O atom and one ^{18}O atom, while a $^{16}O_2$ molecule would give two ^{16}O atoms.

Finally, the reaction term in Eq. (5) is given by:

$$\begin{cases} \left(\frac{dn_{32}}{dt}\right)_{\mathrm{Re}} = \frac{S_m}{2V} kc_{16}^2 \\ \left(\frac{dn_{36}}{dt}\right)_{\mathrm{Re}} = \frac{S_m}{2V} kc_{18}^2 \\ \left(\frac{dn_{34}}{dt}\right)_{\mathrm{Re}} = \frac{S_m}{V} kc_{16}c_{18} \end{cases} \quad (10)$$

with:

$S_m = (N_A f_m m_{cat} D) / (c_m M_m)$

where: S_m is the total surface area of the metal nanoclusters in the catalyst, f_m is the metal loading in the catalyst, m_{cat} is the catalyst sample mass, D is the dispersion of the metal nanoclusters (ratio between the number of surface metal atoms to the total number of metal atoms in the nanoclusters), M_m is the molar mass of the metal and V is the reactor volume.

$k = A\exp(-Q/RT)$ is the reaction rate constant ($m^2\,mol^{-1}\,s^{-1}$), n_i and c_i, respectively represent the volume and surface concentrations ($mol\,m^{-3}$ and $mol\,m^{-2}$ respectively), Q is the reaction activation energy ($J\,mol^{-1}$), A ($m^2\,mol^{-1}\,s^{-1}$) is the pre-exponential factor, T is the temperature (K) and R is the universal gas constant.

The term in second brackets gives the uncovered part of metal surface at time t after formed molecules have desorbed from the surface. This amount of oxygen must be added to the amount of already adsorbed oxygen of corresponding isotopes:

$$\begin{cases} c_{16}(t + \Delta t) = c_{16}(t) + \left(\Delta c_{16}(t)\right)_{AD} \\ c_{18}(t + \Delta t) = c_{18}(t) + \left(\Delta c_{18}(t)\right)_{AD} \end{cases}. \quad (12)$$

To keep balance the same amount of oxygen molecules must be removed from the gas phase:

$$\begin{cases} n_{32}(t + \Delta t) = n_{32}(t) - \frac{S_m}{2V}\left(c_m - (c_{16}(t) + c_{18}(t))\right) f_{32}(t) \\ n_{36}(t + \Delta t) = n_{36}(t) - \frac{S_m}{2V}\left(c_m - (c_{16}(t) + c_{18}(t))\right) f_{36}(t) \\ n_{34}(t + \Delta t) = n_{34}(t) - \frac{S_m}{2V}\left(c_m - (c_{16}(t) + c_{18}(t))\right) f_{34}(t) \end{cases}. \quad (13)$$

Finally, the time variation of the concentration in the gas phase of the i-th type of dioxygen molecule in eq. (5) is given by:

$$\begin{cases} \frac{dn_{32}}{dt} = \frac{S_m}{2V} kc_{16}^2 - \left(\frac{dn_{32}}{dt}\right)_{AD} \\ \frac{dn_{36}}{dt} = \frac{S_m}{2V} kc_{18}^2 - \left(\frac{dn_{36}}{dt}\right)_{AD} \\ \frac{dn_{34}}{dt} = \frac{S_m}{V} kc_{16}c_{18} - \left(\frac{dn_{34}}{dt}\right)_{AD} \end{cases}. \quad (14)$$

The terms with index "AD" represents adsorption term expressed by eq.(13).

4.2. Surface Diffusion

Oxygen atoms adsorbed on the metal particles may "jump" onto the oxide surface and further diffuse. To keep the mass balance, it is assumed that the jump of one oxygen atom from the metal to the oxide is balanced by another atomic jump from the oxide to the metal particle. In fact, oxygen atoms do not accumulate on the oxide surface. Initially, there is no ^{18}O atoms in the oxide and the concentration gradient of ^{18}O is very high. As follows from the first Fick's law, ^{18}O atoms move from the nanoclusters to the oxide and this flux is compensated by the flux of ^{16}O atoms from the oxide to the metal surface. Then, the ^{16}O atoms arrived at the metal surface might react with other oxygen atoms and leave the surface as dioxygen molecules. (11)

In order to calculate the gradient of ^{18}O atoms diffusing on the oxide, the surface around the metal particles was virtually divided into square-shaped rings as schematized on Fig. 4. The surface area of these layers weakly depends on the shape of the metal particles. For example, the area of one layer around a cubic or a semi-spherical nanocluster would only differ by a factor of $4/\pi$.

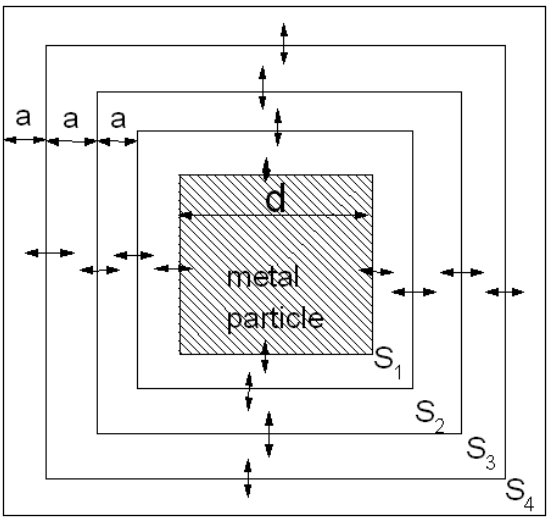

Fig. 4. Square-shaped layers around the metal nanoclusters on the oxide surface

In our case, cubic metal particles were considered. The surface area of *L*-th square-shaped layer is obtained from the following expression:

$$S^{(L)} = 4N(d + (L-1)a)a \ , \qquad (15)$$

where: a is the thickness of one layer, $N = S_m / 5d^2$ is the total number of metal nanoclusters on the catalyst, d is the size of one metal nanocluster.

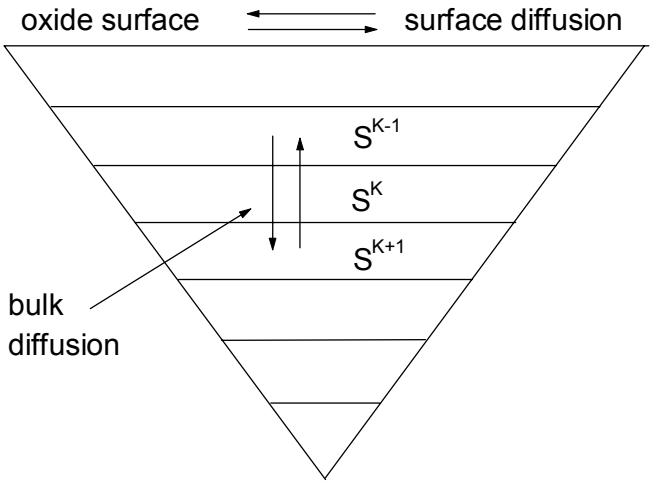

Fig. 5. Scheme of the layers introduced for surface and bulk diffusion calculations

Taking into account (i) the area variation of the layers as a function of the distance from the metal particle and (ii) the different directions of the oxygen atoms fluxes, the time variation of the *i*-th type of atom in the *L*-th surface ($K = 1$) layer (Fig. 5) is obtained from the second Fick's law, considering finite increments:

$$\left(\frac{dc_i^{(1,L)}}{dt}\right)_{SD} = \frac{D_s}{a^2}\left(A^{(L-1)}\left(c_i^{(1,L-1)} - c_i^{(1,L)}\right) - \right.$$

$$\left. - A^{(L)}\left(c_i^{(1,L)} + c_i^{(1,L+1)}\right)\right), \ i = 16, 18 \ , \qquad (16)$$

where:

$$A^{(L)} = \begin{cases} \dfrac{S^{(L+1)}}{S^{(L)}}, if \ \mathrm{c_i^{(L)} - c_i^{(L+1)} \geq 0} \\ \dfrac{S^{(L)}}{S^{(L+1)}}, if \ \mathrm{c_i^{(L)} - c_i^{(L+1)} < 0} \end{cases} .$$

Eq. (16) is also valid for oxygen jumps from/to the metal particles ($L = 0$). For layer $L = 0$ Eq. (16) is given by:

$$\left(\frac{dc_{18}}{dt}\right)_S = -\frac{D_S}{a^2}\left(c_{18} - c_{18}^{(1,1)}\right)A^{(0)} = -\left(\frac{dc_{16}}{dt}\right)_S \ , \qquad (17)$$

where $c_{18}^{(1,1)}$ is the concentration of ^{18}O atoms diffusing on the oxide surface in the first layer around metal nanoclusters, a is the length of atomic jump equal to lattice parameter.

The number of rings (L) around the metal particle is not infinite but limited either by the mean distance between metal particles or by the oxide grain size. The mean distance (x_L) between metal particles is obtained from the expression:

$x_m = (S_{ox} / N)^{1/2}$

and the number of layers is given by:

$L = 0.5 x_m / a$,

where S_{ox} is the total surface of the oxide.

However, for some catalysts, x_m can be higher than the oxide grain size (d_{ox}) and in this case:

$L_{max} = 0.5 d_{ox} / a$.

4.3. Bulk Diffusion

Oxygen atoms diffusing on the surface of the oxide may also diffuse into the bulk of the oxide grain (Fig. 6). To determine the concentration gradients in the bulk of the oxide, oxide layers (K) with a thickness h were introduced. However, considering powder catalysts with cubic shape grains it is necessary to take into account the fact that the area of each layer ($S^{(K)}$) decreases and tends to zero as one goes deeper and deeper into the oxide bulk. So, these areas were calculated according to the following expression:

$$S_B^{(K)} = S_{ox}\left(1 - 2(K-1)h / d_{ox}\right)^2 . \qquad (18)$$

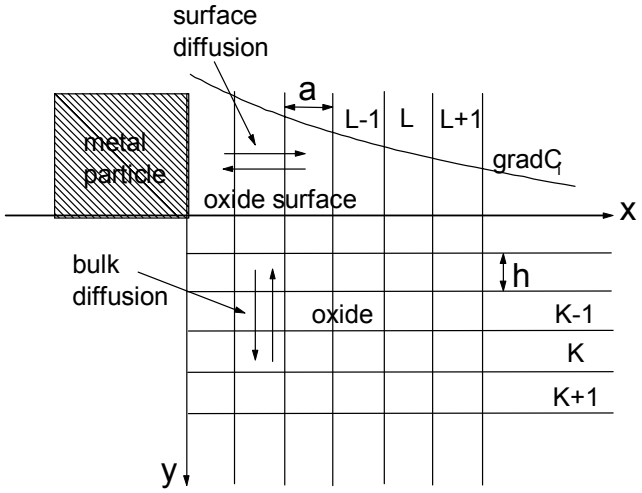

Fig. 6. Arrangement of the monolayers in a cubic oxide grain of a powder catalyst

The variation of the atomic concentration in oxygen atoms in one given layer K of the oxide is calculated

according to the second Fick's law, in a similar way to surface diffusion.

Taking into account the different fluxes, the variation of the concentration of the *i*-th type of oxygen atom in the *K*-th bulk layer and in the *L*-th surface ring takes the following form:

$$\left(\frac{dc_i^{(L,K)}}{dt}\right)_{SD} = \frac{D_b}{h^2}\left(B^{(K-1)}\left(c_i^{(L,K-1)} - c_i^{(L,K)}\right) - B^{(K)}\left(c_i^{(L,K)} + c_i^{(L,K+1)}\right)\right), \quad (19)$$

where

$$B^{(K)} = \begin{cases} \dfrac{S^{(K+1)}}{S^{(K)}}, if\ c_i^{(L,K)} - c_i^{(L,K+1)} \geq 0 \\ \dfrac{S^{(K)}}{S^{(K+1)}}, if\ c_i^{(L,K)} - c_i^{(L,K+1)} < 0 \end{cases}.$$

4.4. Direct Exchange between the Gas Phase and Binuclear Species Present on the Oxide Surface

To take into account direct exchange between the gas phase and binuclear species, which exist on the oxide surface, the following reactions, occurring at the interface between the gas phase and – the oxide surface, were considered [6]:

$$^{18}O^{18}O_g + {}^{16}O^{16}O_s = {}^{18}O^{18}O_s + {}^{16}O^{16}O_g\ ;$$
$$^{16}O^{16}O_g + {}^{18}O^{18}O_s = {}^{16}O^{16}O_s + {}^{18}O^{18}O_g\ . \quad (20)$$

The corresponding rate equations for the variation of the $^{16}O_2$ and $^{18}O_2$ surface molecular concentrations upon direct exchange are:

$$\left(\frac{dc_i}{dt}\right)_{sup} = k_{sup}\frac{V}{S_{ox}}\left(n_i c_j - n_j c_i\right), \quad i,j = 32, 36\ , \quad (21)$$

where: k_{sup} is the reaction rate constant and c_i, obtained from Eq. (22), is the average concentration in $^{16}O_2$ and $^{18}O_2$ species at the surface of the catalyst.

$$c_i = f_{ox}\frac{1}{2x_N}\sum_{L=1}^{L_{max}} c_p^{(L,1)}\ ,\quad p = 16, 18,\quad i = 32, 36\ , \quad (22)$$

where f_{ox} is the fraction of binuclear oxygen species at the oxide surface.

The corresponding rate equation term for the variation of the oxygen concentration in the gas phase is:

$$\left(\frac{dn_i}{dt}\right)_{sup} = k_{sup}\left(n_i c_j - n_j c_i\right), \quad i,j = 32, 36\ . \quad (23)$$

Upon simulation, this term might be added to Eq. (5) whenever direct exchange should be included. If such a process occurs, the oxygen composition at the surface is changed and surface and bulk diffusion is influenced. Then, it is necessary to recalculate the oxygen isotopes distribution in each surface layer *L*. The time variation of the concentration in oxygen ^{16}O and ^{18}O atoms in the surface layer *L*, following direct exchange, is obtained from the following expression:

$$\left(\frac{dc_r^{(L)}}{dt}\right)_{sup} = 2k_{sup}\frac{V}{x_N S_{ox}}\left(n_i c_j - n_j c_i\right),$$
$$i,j = 32, 36,\quad r = 16, 18\ . \quad (24)$$

5. RESULTS AND DISCUSSION

5.1. $Pt/Ce_xZr_{1-x}O_2$ Catalyst

Kinetics

Experimental kinetic curves of isotopic composition change in gas phase are used as initial data. Fitting of these curves by the above model allows to calculate reaction rates, diffusion coefficients and activation energies. Here the isotopic oxygen exchange in $Pt/Ce_xZr_{1-x}O_2$ powder catalysts is analyzed to test the validity of the model. Experimental results used here are taken from Ref. [16], where catalyst preparations and their characteristics are detailed.

Experimental results presented in Figs. 7 and 8 (points) show that oxygen spillover takes place. Although pure $^{18}O_2$ was initially introduced in gas phase, $^{16}O_2$ and $^{18}O^{16}O$ progressively appear in the reactor gas phase. Whatever the steps involved in exchange (surface and bulk diffusion, direct exchange with oxide surface) the oxygen

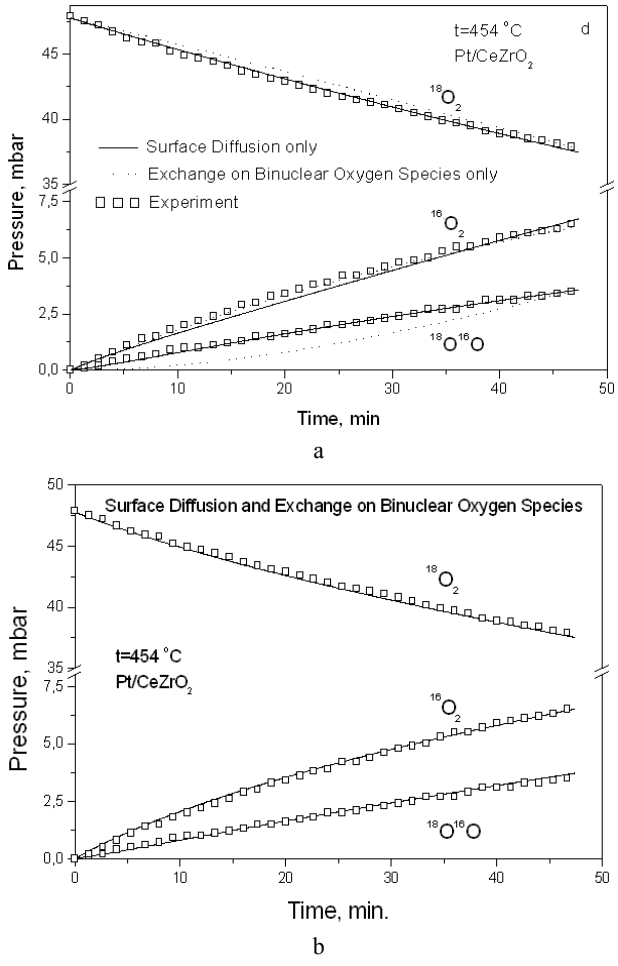

Fig. 7. Experimental and fitted curves of time dependencies of oxygen partial pressure in gas phase during oxygen exchange on $Pt/Ce_xZr_{1-x}O_2$ catalyst at $t = 454$ °C: a) separating surface diffusion and exchange on binuclear oxygen species processes and b) including both processes in calculations

isotope ^{16}O can only be taken from the solid. Fig. 7, a, shows fitting results including the processes of surface diffusion (solid lines) and of exchange on binuclear oxygen species (dot lines), separately (exchange on metal nanoparticles is always included). In calculations with participation of binuclear oxygen species it is assumed that their fraction is 10 % of the total amount of surface oxygen in support [9]. Kinetic curves for oxygen $^{18}O_2$ and $^{16}O_2$ are quite well fitted in both cases, however, the curve for $^{18}O^{16}O$ in the case of exchange on binuclear oxygen species shows a qualitatively different behavior. It seems that this process was not preeminent. Considering the fitting in the case of surface diffusion, the results are in a good agreement for all three curves, although the previous fit with exchange on binuclear species was a little better for curve $^{16}O_2$. Apparently, the two processes, surface diffusion and direct exchange of binuclear species have to be considered to proceed simultaneously. Fig. 7, b, shows the excellent fitting obtained in this case and shows that exchange essentially proceeds via adsorption, recombination and desorption on metal clusters and surface diffusion on oxide while the direct exchange on binuclear oxygen species has significant influence on exchange rates and diffusion coefficients. The calculated values of these parameters for the three different fitting cases are summarized in Table 1.

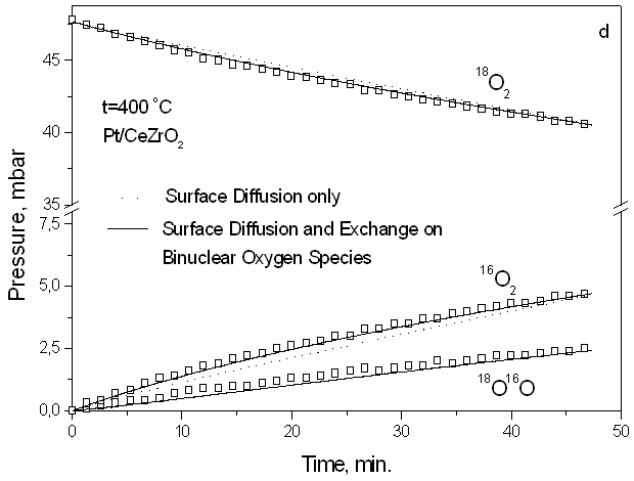

Fig. 8. Experimental and fitted curves of time dependencies of oxygen partial pressure in gas phase during oxygen exchange on $Pt/Ce_xZr_{1-x}O_2$ catalyst at $t = 400$ °C including in calculations surface diffusion with and without exchange on binuclear oxygen species

The rate of exchange on metal particles k varies by a factor of 2 and diffusion coefficient D_s by factor of 10. Obviously, the process of direct exchange on support changes the surface morphology and has a direct impact on oxygen diffusivity. This decrease in surface diffusion coefficient can be explained by the fact that a part of the ^{16}O appearing in gas phase comes from oxide via a direct exchange on binuclear oxygen species without any participation of metal clusters and surface diffusion. The same explanation can be given for changes in reaction rate of exchange on metal clusters. In the absence of exchange on binuclear oxygen species, the whole ^{16}O atoms appearing in gas phase come integrally from desorption from metal clusters. The same behavior is observed for experimental results obtained at other temperatures.

In Fig. 8 experimental (points) and calculated (lines) are presented including both processes, surface diffusion and exchange on binuclear oxygen species, obtained at temperature $t = 400$ °C. Calculations performed at lower temperatures (303, 334, 359, 370 °C, results not presented here) showed the same behavior.

Activation energies

Arrhenius plots of exchange rate constants (k) on metal clusters in the two different cases: with and without exchange on binuclear oxygen species are presented on Fig. 9. Both lines are close to each other and a small difference of the slope is observed. The activation energy of exchange on metal clusters decreases from 71 kJ/mol to 67 kJ/mol when binuclear oxygen species can intervene in the whole process. Other processes cannot affect the activation energy of exchange on metal clusters. Therefore, the decrease of activation energy when the direct exchange on binuclear oxygen species can occur would mean that this process should be integrated in the global oxygen exchange on ceria-zirconia-supported platinum catalysts.

Arrhenius plot for reaction rate constant of exchange on binuclear oxygen species is presented in Fig. 10. The activation energy (97 kJ/mol) is higher than for exchange via metal clusters. It follows that this process can be ignored at low temperature.

The Arrhenius plot for surface diffusion coefficients is presented in Fig. 11. The activation energy (113 kJ/mol) is in fair agreement with values obtained for similar catalysts [12] by simple methods previously proposed by Holmgren [17] Kramer [13] and Kakioka [14].

Table 1 Values of exchange rate constant on metal particles k, surface diffusion coefficient D_s and exchange rate constant on binuclear oxygen species k_{sup} obtained after fitting of experimental data at $t = 454$ °C (Figs. 7 and 8) for different processes.

Processes	Reaction rate constant on metal clusters k ($m^2mol^{-1}s^{-1}$)	Surface diffusion coefficient D_s ($\times10^{-20}$, m^2s^{-1})	Reaction rate constant on binuclear oxygen species k_{sup} ,($m^2mol^{-1}s^{-1}$)
Surface diffusion (Fig. 10, a, solid line)	1517	90	–
Exchange on binuclear oxygen species (Fig. 12, a, dot line)	3571	–	62
Surface diffusion and exchange on binuclear oxygen species (Fig. 12, b)	1071	9	49

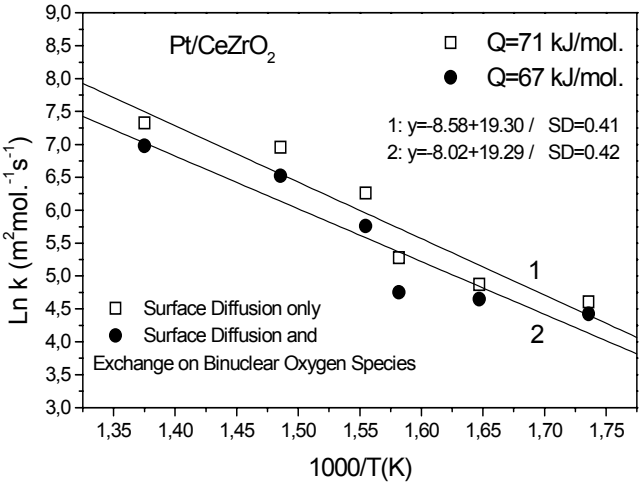

Fig. 9. Arrhenius plot of oxygen exchange rate constant on Pt clusters including surface diffusion with and without exchange on binuclear oxygen species. SD is a standard deviation of the fit

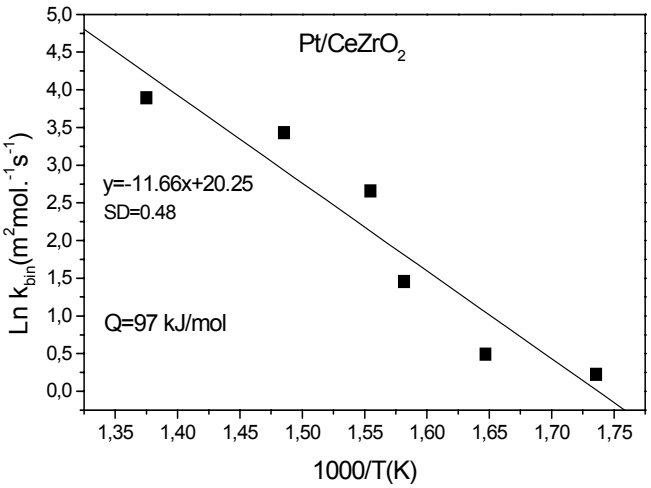

Fig. 10. Arrhenius plot of oxygen exchange rate constant on binuclear oxygen species

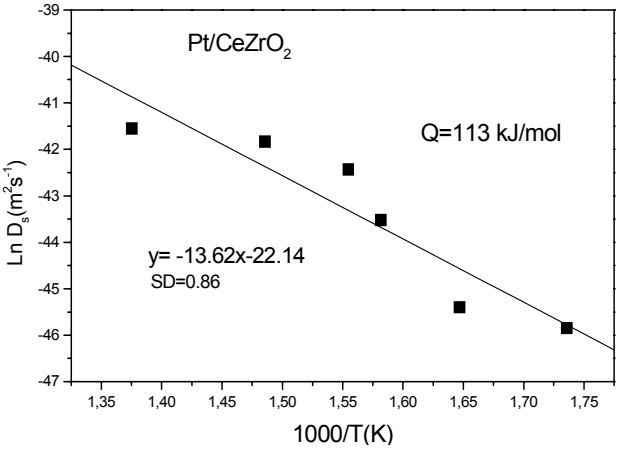

Fig. 11. Arrhenius plot of surface diffusion coefficient

For example, an activation energy of 72 kJ/mol was found for oxygen exchange on Pt/CeO_2 catalyst between 330 °C and 410 °C and a surface diffusion coefficient of 78×10^{-19} m^2s^{-1} was found for oxygen on Rh/CeO_2 at 400 °C (compare results on Figs. 7 and 8 and Table 1). However, these simple methods are based only on initial rates of exchange and cannot represent the global process as good as with the present model which integers all the experimental data over one hour of exchange.

Surface composition

For a better understanding of the mechanism of exchange, time dependencies of concentrations of oxygen isotopes on the surface of catalyst are presented in Figs. 12 and 13. These values were calculated when fitting the curves presented in Fig. 7, a, (case of surface diffusion only). In Fig. 12, the main window shows the composition evolution on metal clusters during all processing time (0 min – 50 min). The small window shows the composition changes during the first second of exchange. As there is initially no oxygen ^{16}O in gas phase, the metal surface is covered only by ^{18}O isotopes at the very beginning of reaction.

During the first seconds, ^{18}O concentration quickly decreases because of the diffusion from metal to oxide surface. This flux is balanced by the flux of ^{16}O from oxide to metal clusters. The isotopic distribution shows an interesting behavior: it quickly passes through the extrema values (^{16}O maximum and ^{18}O minimum) and then slowly approaches the steady state. The appearance of minimum and maximum concentrations of isotopes during exchange is not unusual. Such behavior is always observed in kinetic curves at non-steady state regime when at least two different driving forces act in the system [18, 19]. In this case, there are fluxes at interface metal-oxide and at interface gas-metal, produced by the processes of adsorption-desorption and surface diffusion, which generate the perturbation in the system at initial stages.

At $t \approx 10$ min. the concentration curves in Fig. 12 approach the steady state regime, which means that stable concentration gradients are then established on the surface of oxide. The calculated concentration gradients of isotope ^{18}O at different times are presented in Fig. 13. The abscissa represents the mean distance between the metal cluster periphery ($L = 0$) and a point of the oxide surface. This figure confirms that at $t = 10$ min. the stable concentration gradient in surface layer is reached and only weak changes are further observed (curve 5). Stable concentration gradient gives continuous increase of the amount of oxygen isotope ^{16}O in gas phase. It follows that the process of surface diffusion is predominant during the whole exchange time.

The time dependencies of the oxygen atomic ^{18}O (^{16}O) flux crossing the total perimeter of metal clusters are presented in Fig. 14. At $t < 1$ min. the flux is very high and then rapidly decreases. At the later stages it slowly decreases but remains far from being nil. This behavior is not systematically observed and may depend on sample preparation. There are many experimental measurements where a steady-state of partial pressures in gas phase can be observed [12]. In those cases the flux at saturation becomes virtually nil, which means that the diffusion coefficient may decrease during process [20]. In the calculations presented above, the diffusion coefficient was kept as constant during the whole processing time. However, for samples showing a quasi-equilibrium behavior before the end of experiment, the best fitting requires to introduce time dependence for the diffusion coefficient [21].

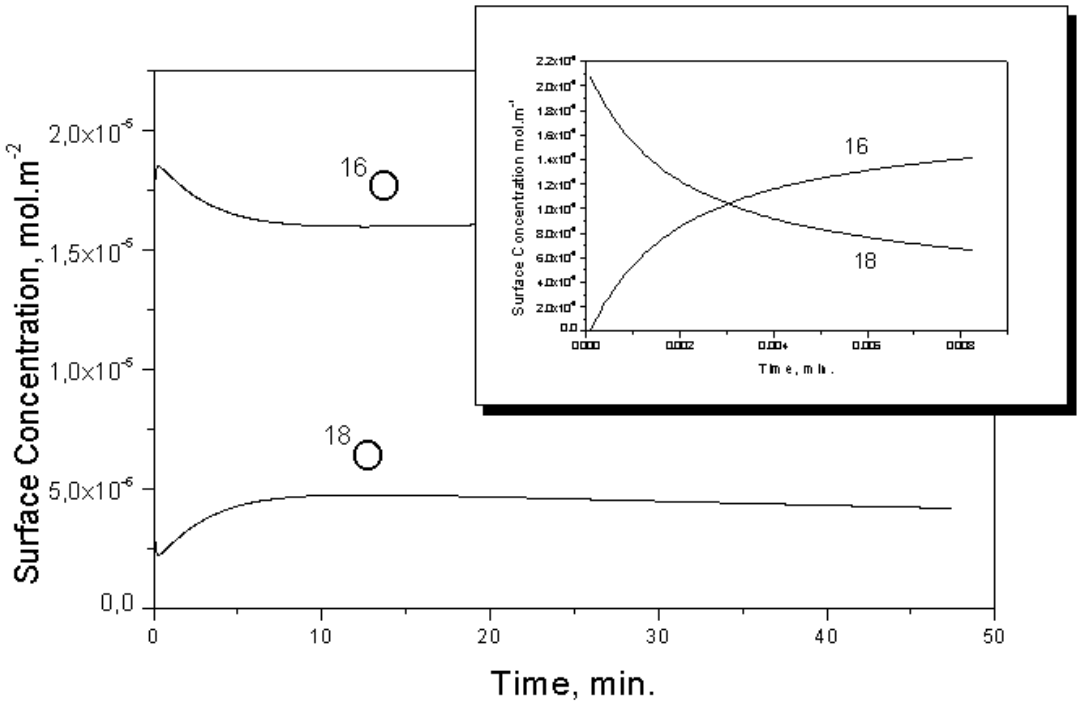

Fig. 12. The time dependencies of oxygen isotopes ^{16}O and ^{18}O adsorbed on metal particles. The main window shows the composition variation during all processing time and the smaller one shows the same but during the first second

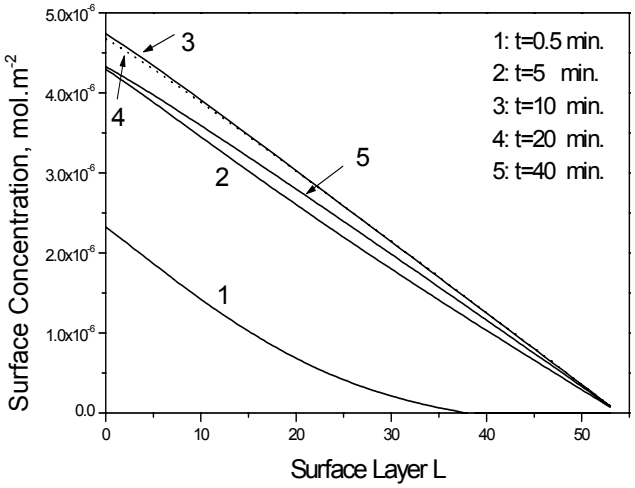

Fig. 13. The distribution of oxygen isotope ^{18}O on the surface of oxide as a result of surface diffusion at different moments of processing time

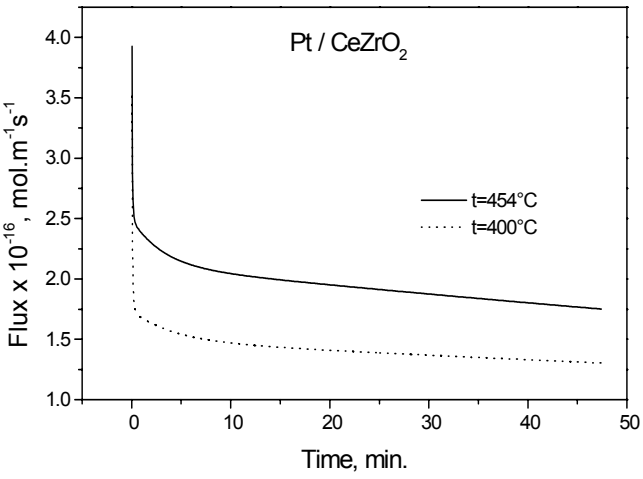

Fig. 14. The time dependencies of the oxygen atom flux crossing the total perimeter of metal particles calculated at different temperatures

Bulk diffusion

Considering the process of bulk diffusion, there are difficulties to find any qualitative feature in experimental kinetic curves of gas phase partial pressure which can be unambiguously linked to bulk diffusion (at least in the result of Figs. 7 and 8). As a rule, this is an unsolved problem that may arise because such kinetic curves contain information about the amount of oxygen, which crosses the interface metal-oxide [22]. Unfortunately, these atoms may originate from the surface as well as from the bulk of oxide. The correct answer to this problem could only be given by additional measurements of elemental composition using other methods (e. g. SIMS depth profiling).

The method allowing to discriminate contribution of surface and bulk diffusion in partial pressure kinetic curves of gas phase was previously proposed by Kakioka [14]. However, this method is based on the assumption that at the complete exchange of oxygen on the surface is achieved before the exchange in deeper layers takes place. The bulk diffusion coefficients obtained by this method were between 3 to 4 orders of magnitude less than surface diffusion coefficient [12]. For samples considered here, as it is seen in Fig. 14 the surface is neither completely exchanged during the time of measurement. Additional calculations showed that during measurement time 25.5 μmol of oxygen ^{18}O were exchanged while initially

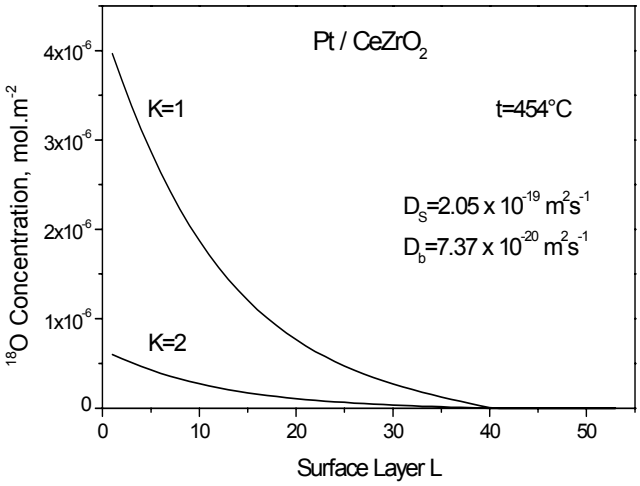

Fig.15. The distribution of oxygen isotope ^{18}O on the surface of oxide $K = 1$ and in second monolayer $K = 2$ as a result of surface diffusion including contribution of bulk diffusion at processing time $t = 40$ min.

there were 36.7 μmol of oxygen ^{16}O on the surface of support oxide. Although good fittings were obtained without any contribution of bulk diffusion (see Figs. 7 and 8), the model with bulk diffusion was performed for samples of Fig. 7. The curves fitted by this model were very close to those presented in Fig. 7 (solid lines). However, the elemental distribution on the surface of oxide is significantly different. The results are presented in Fig. 15 where the distribution of ^{18}O at $t = 40$ min. in the first (surface) $K = 1$ and second $K = 2$ (subsurface) monolayers along the L-axis (surface of support) are presented. Fig. 15 shows that some amount of ^{18}O penetrates into the bulk of oxide. This penetration is deeper near the metal clusters. Calculated values for both surface and bulk diffusion coefficients are presented in Fig. 15. Note that the value of surface diffusion coefficient decreases from (9×10^{-19}) m^2s^{-1} in the absence of bulk diffusion to (2×10^{-19}) m^2s^{-1} with bulk diffusion. The concentration distribution on the oxide surface (curve $K = 1$ of Fig. 15) can be compared with curve 5 of Fig. 13 as both are calculated at the same time. In Fig. 13 (without bulk diffusion) the concentration of ^{18}O almost linearly decreases with distance from metal cluster. In Fig. 15 (with bulk diffusion) the same curve decreases exponentially and seems to be more realistic. This means that bulk diffusion takes place at least for samples considered here and can play a significant role. Calculated values of bulk diffusion coefficient are by one order of magnitude less than those of surface diffusion. New calculations were performed with bulk diffusion coefficient forced to be 4 orders of magnitude less than surface diffusion coefficient. They showed that the distribution on the surface was very similar to those of Fig. 18. However, simulations made with other samples (e. g. $Rh/Ce_xZr_{1-x}O_2$ [21]), diffusion coefficients remained 2 – 4 orders of magnitude less than coefficient of surface diffusion. Nature of metal as well as pretreatment of the catalysts can significantly affect the relative values of the bulk diffusion coefficient. Further works are presently in progress to elucidate this behavior of ceria-zirconia-supported noble metal catalysts.

5.2. Rh/CeO_2 Catalyst

In Figs. 16 – 18, the experimental results, obtained upon heteroexchange on a Rh/CeO_2 sample, are presented. At the beginning of the reaction, only dioxygen $^{18}O_2$ is introduced in the gas phase. Experimental results show that, upon exchange, dioxygen molecules $^{16}O_2$ and $^{16}O^{18}O$ also appear in the gas phase. It clearly indicates that ^{16}O atoms from the oxide do participate in the reaction. In fact, at the same time as exchange on metal nanoclusters occurs, surface diffusion and/or direct exchange also takes place. The first process is much more likely to occur, while the second one should take place at higher temperatures [23]. However, the correct answer is obtained only after several tries to fit the experimental curves, looking for the best result. Finally, one may observe that bulk diffusion takes place only after surface diffusion occurred, when a significant part of the surface oxygen atoms has been exchanged [14].

The experimental results were tentatively fitted, including only two processes: 1) exchange on the metal nanoclusters and 2) surface diffusion. One can observe that the fitting is quite good at the beginning, but some deviations appear later on. Calculations showed that this deviation couldn't be overcome by including bulk diffusion or direct exchange. Theoretical curves showed higher exchange yield than the experimental results. This means that, during the reaction, the exchange is getting slower. Furthermore, we observed that this deviation increases monotonously with time. This indicates that the exchange rate is not constant but decreases with time. This could be explained if the properties of the catalyst (oxidation state of the metal nanoparticles, stoichiometry of the oxide, etc.) change with time on stream, that is some kind of deactivation. It follows that the reaction rate constants and the surface diffusion coefficient also change with time. Assuming exponential time dependence for the deactivation process, the following expressions for the reaction rate constant and the surface diffusion coefficient were considered:

$$R = R_o(n + m * \exp(t/\tau_1)), \quad n + m = 1; \tag{25}$$

$$D_s = D_{so} * \exp(t/\tau_2) .$$

The fitted results, introducing Eq. (25), are presented in Figs. 17 and 18 for heteroexchange reactions respectively carried out at 311 °C and 270 °C on a Rh/CeO_2 sample. In that case, both fittings are optimum over whole reaction time. As good fittings were also obtained for experimental curves registered for heteroexchange reactions carried out on the same catalyst at 256, 279 and 327 °C (not presented here).

Evolutions as a function of temperature of the calculated values for the reaction rate constants and the surface diffusion coefficients are displayed (Arrhenius plot) in Figs. 19 and 20, respectively. Fitting the calculated points to a line gives access to the activation energies for the different processes. Activation energies are $Q = 75.4$ kJ/mol for the exchange on the metal particles and $Qs = 27.0$ kJ/mol for the surface diffusion. These values are in good agreement with the data available in the literature [12, 17, 23].

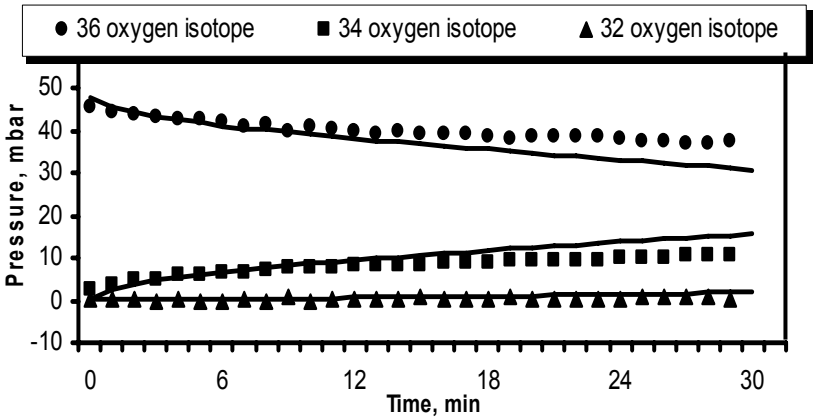

Fig. 16. Experimental and fitted (R = const, D = const.) results of the kinetic curves upon heteroexchange at t = 311 °C on a Rh/CeO_2 catalyst

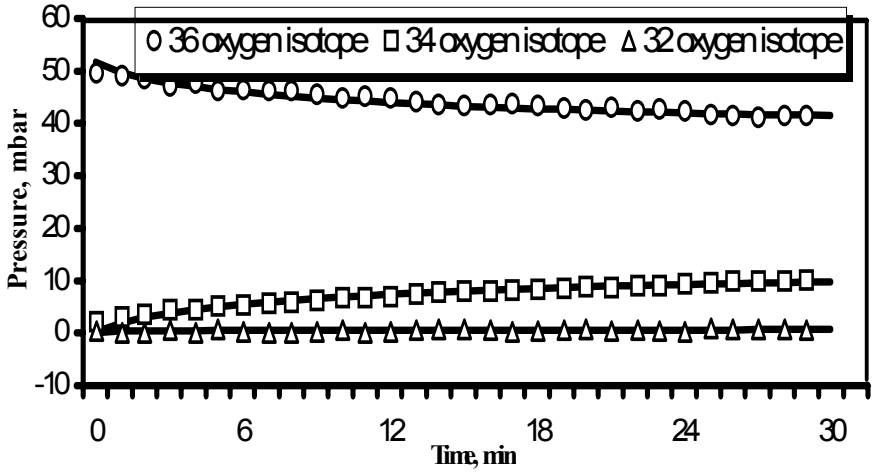

Fig. 17. Experimental and fitted ($R \neq$ const, $D \neq$ const) results of the kinetic curves upon heteroexchange on a Rh/CeO_2 catalyst at t = 278 °C

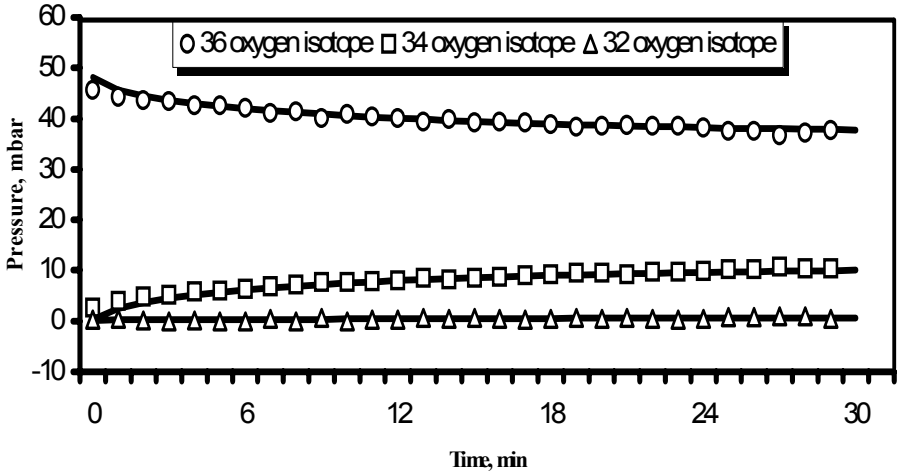

Fig. 18. Experimental and fitted ($R \neq$ const, $D \neq$ const) results of the kinetic curves upon heteroexchange on a Rh/CeO_2 catalyst at t = 311 °C

One can notice that the fittings of the experimental curves were good enough, even without including bulk diffusion. This was not surprising if one consider what is known about oxygen diffusion on ceria. In fact, oxygen was shown to be poorly mobile in the bulk of ceria compared to ceria-zirconia mixed oxides. Furthermore, from the experimental results one can only state that ^{16}O atoms diffuse from the oxide to the metal nanoparticles and then desorb as dioxygen molecules. Unfortunately, it is impossible to say from which oxide layer (L,K) ^{16}O atoms come. Only in the case where all surface oxygen atoms would be exchanged (50 % ^{16}O – 50 % ^{18}O), the kinetic

curves would show qualitative differences. In our case in fact, the surface area of the catalyst is so high that such a surface exchange level is never reached.

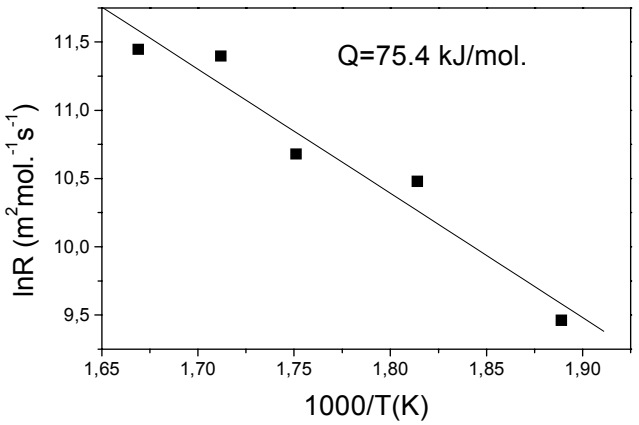

Fig. 19. Arrhenius plot for the reaction rate constant on the metal particles for Rh/CeO_2

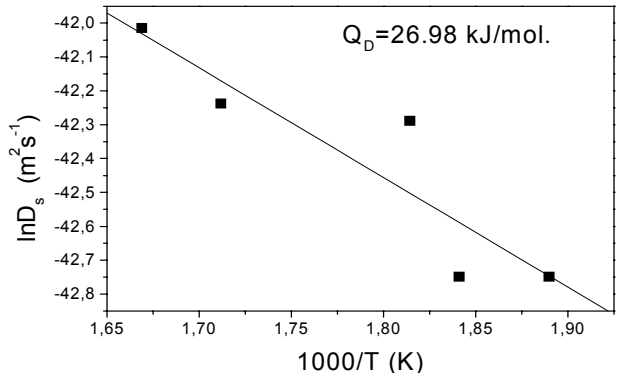

Fig. 20. Arrhenius plot for the surface diffusion coefficient for Rh/CeO_2

6. CONCLUSIONS

1. The most complete kinetic model presented here for oxygen isotopic exchange on oxide supported metal catalysts leads to a good fit between experimental and calculated kinetic curves. Model is based on two very important points: 1) the parallel calculation of surface and bulk diffusion and 2) the implication of certain O species such as superoxides. There is a rather good agreement between kinetic and thermodynamic parameters estimated by the model and those determined by other methods.

2. The main processes taking place upon oxygen heteroexchange on a Rh/CeO_2 catalyst are the dissociative adsorption – desorption of dioxygen on the metal nanoparticles and the surface diffusion on the oxide. Surface ^{16}O atoms are exchanged with diffusing ^{18}O atoms coming from the surrounding gas phase. The formation of new dioxygen molecules and the desorption only take place on the metal nanoparticles.

3. The main processes during oxygen exchange on $Pt/Ce_xZr_{1-x}O_2$ catalyst are exchange on metal clusters and surface diffusion. Direct exchange on binuclear oxygen species as well as bulk diffusion has not an excessive influence in the 200 °C – 450 °C temperature range but cannot be ignored, especially at the highest temperatures.

4. The problem how to discriminate surface and bulk diffusion by measuring composition changes in gas phase remains unsolved. However, the model allows to calculate reasonable values for the surface and bulk coefficients, which otherwise could not be made by any other model. Time-dependent ^{18}O compositions on the metal, at the oxide surface and in the bulk as well as oxygen fluxes at the metal particle periphery can also be calculated.

5. In the interval between 250 °C and 330 °C, for Rh/CeO_2 the activation energy for the dioxygen activation on the metal nanoparticles is $Q = 75.4\ \mathrm{kJ\,mol^{-1}}$ and the activation energy for oxygen atoms surface diffusion is $Q_s = 27.0\ \mathrm{kJ\,mol^{-1}}$. At the same time, surface diffusion coefficient varies from $2.7\times10^{-19}\ \mathrm{m^2\,s^{-1}}$ to $5.7\times10^{-19}\ \mathrm{m^2\,s^{-1}}$.

6. In the 200 °C – 450 °C range of temperatures the activation energy for oxygen exchange on $Pt/Ce_xZr_{1-x}O_2$ catalyst is $71\ \mathrm{kJ\,mol^{-1}}$ and preexponential term in Arrhenius equaton is equal to $2.1\times10^{8}\ \mathrm{m^2\,mol^{-1}s^{-1}}$. Activation energy of surface diffusion $Q_s = 113\ \mathrm{kJ\,mol^{-1}}$ and preexponential term is equal to $2.8\times10^{-10}\ \mathrm{m^2\,s^{-1}}$.

REFERENCES

1. **Kašpar, J., Fornasiero, P., Graziani, M.** Use of CeO_2-based Oxides in the Three-way Catalysis *Catal. Today* 50 1999: p. 285.
2. **Zhdanov, V. P., Kasemo, B.** Kinetic Models of Oxygen Supply from CeO_x to Active Nanometer Particles of Three-way Catalysts *Appl. Surf. Sci.* 135 1998: p. 297.
3. **Henry, C. R.** Surface Studies of Supported Model Catalysts *Surf. Sci. Rep.* 31 1998: p. 235.
4. **Duprez, D.** In Spillover and Migration of Surface Species on Catalysts. Ed. By Can Li and Qin Xin. *Stud. Surf. Sci. Catal.* 112 1997: p. 13.
5. **Piccalo, L., Henry, C. R.** Molecular Beam Study of the Adsorption and Dissociation of NO on Pd Clusters Supported on MgO(100) *Surf. Sci.* 452 2000: p. 198.
6. **Madier, Y., Descorme, C., Le Govic, A. M., Duprez, D.** Oxygen Mobility in CeO_2 and $Ce_xZr_{(1-x)}O_2$ Compounds: Study by CO Transient Oxidation and $^{18}O/^{16}O$ Isotopic Exchange *J. Phys. Chem. B* 103 1999: p. 10999.
7. **Henry, C. R.** Catalytic Activity of Supported Nanometer-sized Metal Clusters *Appl. Surf. Sci.* 164 2000: p. 252.
8. **Schubert, M. M., Hackenberg, S., Van Veen, A. C., Muhler, M., Plazak, V., Behm, R. J.** CO Oxidation over Supported Gold Catalysts – "Inert" and "Active" Support Materials and Their Role for the Oxygen Supply during Reaction *J. Catal.* 197 2001: p. 113.
9. **Descorme, C., Madier, Y., Duprez, D.** Infrared Study of Oxygen Adsorption and Activation on Cerium–Zirconium Mixed Oxides *J. Catal.* 196 2000: p. 167.
10. **Descorme, C., Duprez, D.** Oxygen Surface Mobility and Isotopic Exchange on Oxides: Role of the Nature and the Structure of Metal Particles *Appl. Catal. A: General* 202 2000: p. 231.
11. **Fernandez-Garcia, M., Marinez-Arias, A., Iglesias-Juez, A., Belver, C., Hungri, A. B, Conesa, J. C., Soria, J.** Structural Characteristics and Redox Behavior of CeO_2–ZrO_2/Al_2O_3 Supports *J. Catal.* 194 2000: p. 385.
12. **Madier Y.** *PhD Thesis,* Poitiers University, 1999.
13. **Kramer, R., Andre, M.** Adsorption of Atomic Hydrogen on Alumina by Hydrogen Spillover *J. Catal.* 58 1979: p. 287.

14. **Kakioka, H., Ducarme, V., Teichner, S. T.** Isotope Exchange of Oxygen-18 in Carbon Dioxide with the Oxygen Ions in Vanadium(V) Pentoxide *J. Chim. Phys.* 68 1971: p. 1722.
15. **Galdikas, A.** Thin Film Deposition onto the Rough Surface: Phenomenological Investigations *Thin Solid Films* 418 2002: p. 112.
16. **Galdikas, A., Descorme, C., Duprez, D., Dong, F., Shinjon, H.** In Preprints Vol. 3 of Sixth International Congress on Catalysis and Automotive Pollution Control CAPOC 6, Brussels, October 2003: pp. 635 – 645.
17. **Holmgren, A., Duprez, D., Andersson, B.** A Model of Oxygen Transport in Pt/Ceria Catalysts from Isotope Exchange *J. Catal.* 182 1999: p. 441.
18. **Galdikas, A., Pranevičius, L., Templier, C.** Sputtering Induced Roughening Effects on Ion Beam Profiling of Multilayers *Surface Science* 349 (3) 1996: p. 333.
19. **Galdikas, A. Pranevičius, L.** Interaction of Ions with a Condensed Matter. NOVA Science Publishers, Inc, Huntington, New York, 2000: 176 p.
20. **Galdikas, A., Descorme, C., Duprez, D.** Surface Diffusion upon Oxygen Isotopic Exchange on Oxide-supported Metal Nanoclusters *Solid State Ionics* 166 2004: p. 147.
21. **Galdikas, A., Duprez, D., Descorme, C.** (paper in preparation).
22. **Wolf, D., Heber, M., Grunert, W., Muhler, M.** Predictions of Relationships between Catalytic and Solid Phase Properties by Kinetic Models and Their Validation *J. Catal.* 199 2001: p. 92.
23. **Descorme, C., Madier, Y., Duprez, D., Birchem, T.** In Proceedings of 12TH International Congress on Catalysis ed. by **A. Corma et al.** *Stud. Surf. Sci. Catal.* 130 2000: p. 347.

DOI: 10.5755/j02.ms.26330